The structural framework for Carlin-type gold mineralization in the Nadaleen trend, Yukon

A. Steiner*, K. Hickey
Mineral Deposit Research Unit (MDRU), University of British Columbia

A.B. Coulter
Archer Cathro (1981) and Associates Limited

Steiner, A., Hickey, K. and Coulter, A.B., 2018. The structural framework for Carlin-type gold mineralization in the Nadaleen trend, Yukon. *In:* Yukon Exploration and Geology 2017, K.E. MacFarlane (ed.), Yukon Geological Survey, p. 139-149.

ABSTRACT

Structure imparts a significant control on the distribution of Carlin-type gold mineralization recently discovered in the Nadaleen trend, Yukon. An improved understanding of the structural framework for gold mineralization is essential for continued exploration success and interpreting ore fluid controls. Structural observations from the Osiris cluster of the Nadaleen trend indicate that NW-verging F_1 folds were refolded in response to later SSW-NNE directed contraction. F_2 folds have a subvertical ESE-striking axial plane with subvertically plunging axes on steep F_1 limbs and subhorizontal fold axes in shallow F_1 limbs. F_2 folds have a pervasive axial planar cleavage that is recognized regionally. The steeply dipping Osiris and Nadaleen faults appear to cut all folds. Mineralization is spatially associated with later NW-striking faults in the Conrad zone. Much of the folding within the mineralized Conrad limestone is synsedimentary and its geometry reflects its emplacement as an olistostrome.

* *astein@eoas.ubc.ca*

INTRODUCTION

The Nadaleen trend is an array of Carlin-type gold showings within the eastern extent of ATAC Resources Limited's Rackla Gold property in eastern-central Yukon (Fig. 1; Tucker *et al.*, 2013). It is generally considered to encompass the Osiris cluster in the east, including the Osiris, Sunrise, Ibis and Conrad ore zones, and gold occurrences within the Orion area, including the Pyramid showing and the Anubis cluster (Fig. 1b). Gold mineralization occurs in thin arsenic-rich rims on pyrite and is associated with decalcified and silicified host limestone (Tucker *et al.*, 2013; Tucker, 2015). Siliciclastic rocks are locally mineralized proximal to faults and along lithological contacts between mineralized limestone and adjacent siliciclastic rocks. In all host rocks, mineralization is spatially associated with realgar and orpiment, as well as enrichments in As, Sb, Hg and Tl (Tucker *et al.*, 2013). A deposit overview including examples of mineralization is provided by Coulter *et al*. (2018). Lithology and associated porosity and permeability exert a stratigraphic control in which mineralization is preferentially concentrated within some units and along lithological contacts at all scales. Gold distribution is also controlled by structures, with mineralization occurring in folded rock units, and proximal to fault zones at the deposit scale. At smaller scales, mineralization can be observed in stylolites, veins, minor faults, fault gouges, fracture sets and mesoscopic (metre or tens of metre-scale) fold hinges. A detailed structural understanding of the region is essential for considering structural controls on mineralization and identifying ore fluid pathways.

Building on previous work by Palmer and Kuiper (2017) and Tucker (2015), this paper presents the preliminary results of a new study to assess the role structure played in controlling fluid flow and the spatial distribution of gold mineralization along the Nadaleen trend. It summarizes field observations from the summer of 2017 during which the structure of the Osiris cluster was assessed through detailed surface geological mapping, examination of drill core, and 3D geological modelling. We present an updated geological map of the Osiris cluster, as well as structural observations and initial interpretations.

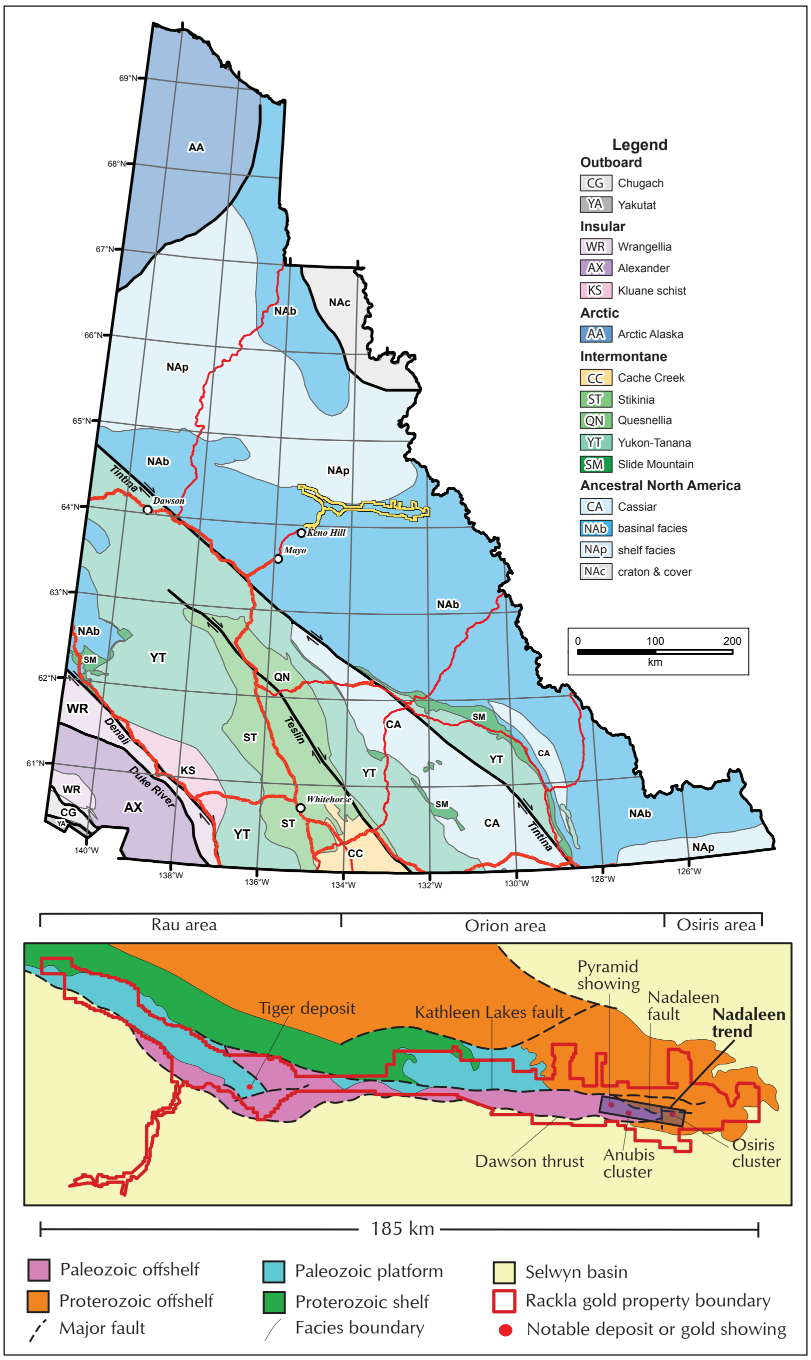

***Figure 1. (a)** Terrane map of Yukon with ATAC Resources Ltd.'s Rackla Gold property outlined in yellow (after Colpron and Nelson, 2011).*
***(b)** Property map with overview geology and the locations of major faults and gold showings (after Colpron et al., 2013). The Nadaleen trend is highlighted in blue.*

SUMMARY OF REGIONAL AND DEPOSIT GEOLOGY

The Nadaleen trend is bound to the north by the Kathleen Lakes fault and to the south by the eastern terminus of the Dawson thrust (Colpron, 2012; Moynihan, 2014). It comprises sedimentary rocks of off-shelf slope to basinal facies that are interpreted as a zone of transitional facies at the interface between the Mackenzie Platform to the north and the Selwyn basin to the south (Colpron, 2012). The Osiris cluster is underlain by Neoproterozoic rocks of the Windermere Supergroup with volumetrically minor mafic intrusive rocks (Tucker *et al.*, 2013), while the Orion area is largely underlain by Palaeozoic sedimentary rocks ranging from Cambrian to Permian in age (Fig. 1b). The Osiris cluster (Fig. 2) is situated in the footwall of the Nadaleen fault, which juxtaposes the Cryogenian Ice Brook Formation against the Nadaleen formation (Fig. 3; Moynihan, 2016).

The Nadaleen formation forms the oldest package of rocks within the Osiris cluster (Moynihan, 2016). The lowermost unit of this formation comprises a thinly bedded silty limestone bound on both sides by a heterogeneous and somewhat chaotic siliciclastic package of sandstone, mudstone and gravel conglomerate. This package is overlain by a black shale unit, which is in turn is overlain by interleaved limestone, rudstone and siliciclastic shale. The Stenbraten member at the top of the Nadaleen formation is a grey argillite that has irregular colour bands of maroon and green in its upper strata. The Gametrail Formation, comprising variably dolomitized silty, quartz-rich limestone and interleaved rudstone, overlies the Nadaleen formation. A calcareous breccia defines the boundary between the Gametrail Formation and overlying Blueflower Formation. The Lower member of the Blueflower Formation is a distinctive thinly bedded brown calcarenite with local conglomerate beds. The overlying Middle member is a well-bedded siltstone with minor limestone beds. This member is overlain by the dolomitized Algae Formation and the maroon coloured Narchilla Formation argillite. Three intrusive igneous rock units have been recognized within the Osiris cluster. The hornblende-rich Osiris gabbro is exposed along Osiris ridge and has been dated as 465.6±4.4 Ma (Tucker, 2015). Two altered dikes have been observed in drill core and in discontinuous surface exposures. They are plagioclase and carbonate-rich with minor pyroxene (Tucker *et al.*, 2013) and have been dated as 74.4±1.0 Ma (Tucker, 2015). More details of Osiris cluster rocks can be found in the map legend (Fig. 2), stratigraphic column (Fig. 3) and in Coulter *et al.* (2018).

The Osiris cluster is generally characterized by steep, homoclinal bedding with monoclines and isolated macroscopic (hundreds of metres in scale or larger) folds. Carbonate units are folded on the mesoscopic and macroscopic scale with only local development of any associated cleavage, and without many smaller scale folds. Less competent argillaceous units accommodate deformation through widespread folding and pervasive cleavage development. Although exposure along ridge-tops is generally excellent for structural analysis, thinly to moderately bedded units tend to be *ex-situ* to some extent as a result of frost-heave and gravitational creep.

SYN-SEDIMENTARY STRUCTURES

Abundant examples of soft sediment deformation and dewatering structures are readily observed in drill core (Fig. 4) from the Nadaleen trend. Examples of soft-sediment structures include soft-sediment folding (Fig. 4a), dewatering dish structures (Fig. 4b), interrupted bedding (Fig. 4b) and convoluted bedding (Fig. 4c). Grain flows (Fig. 4d) and turbidites are also common and are indicative of gravitational instability during deposition. Many of these features, particularly dewatering structures, soft-sedimentary folding and gravity flow deposits, are also observed in surface exposures. Interpreted allochthonous rafts and olistoliths can be observed in the Ice Brook Formation, as well as the Blueflower Formation and the Conrad siliciclastics in the Nadaleen formation (Aitken, 1989, 1991). Mesoscopic synsedimentary slump folds are common in the Osiris cluster and throughout the Orion area. Slump folds are identified within the Upper Osiris limestone, the Conrad siliciclastics and the Conrad limestone (Fig. 5) using the following criteria (after Bradley and Hanson, 1998): 1) folds are anomalous in the wider structural context; 2) folds are disharmonic and variable; 3) folds truncate against one another with no indication of strain along the truncation surface; 4) folds are bound by homoclinal strata or strata recognizable as being tectonically folded from regional events and map contacts do not follow folds; and 5) folds are spatially associated with soft-sediment deformation structures. The best examples of slump folds can be found in the Conrad limestone at 630540 mE, 7112470 mN (Fig. 5; all grid references are relative to the NAD83, UTM8N).

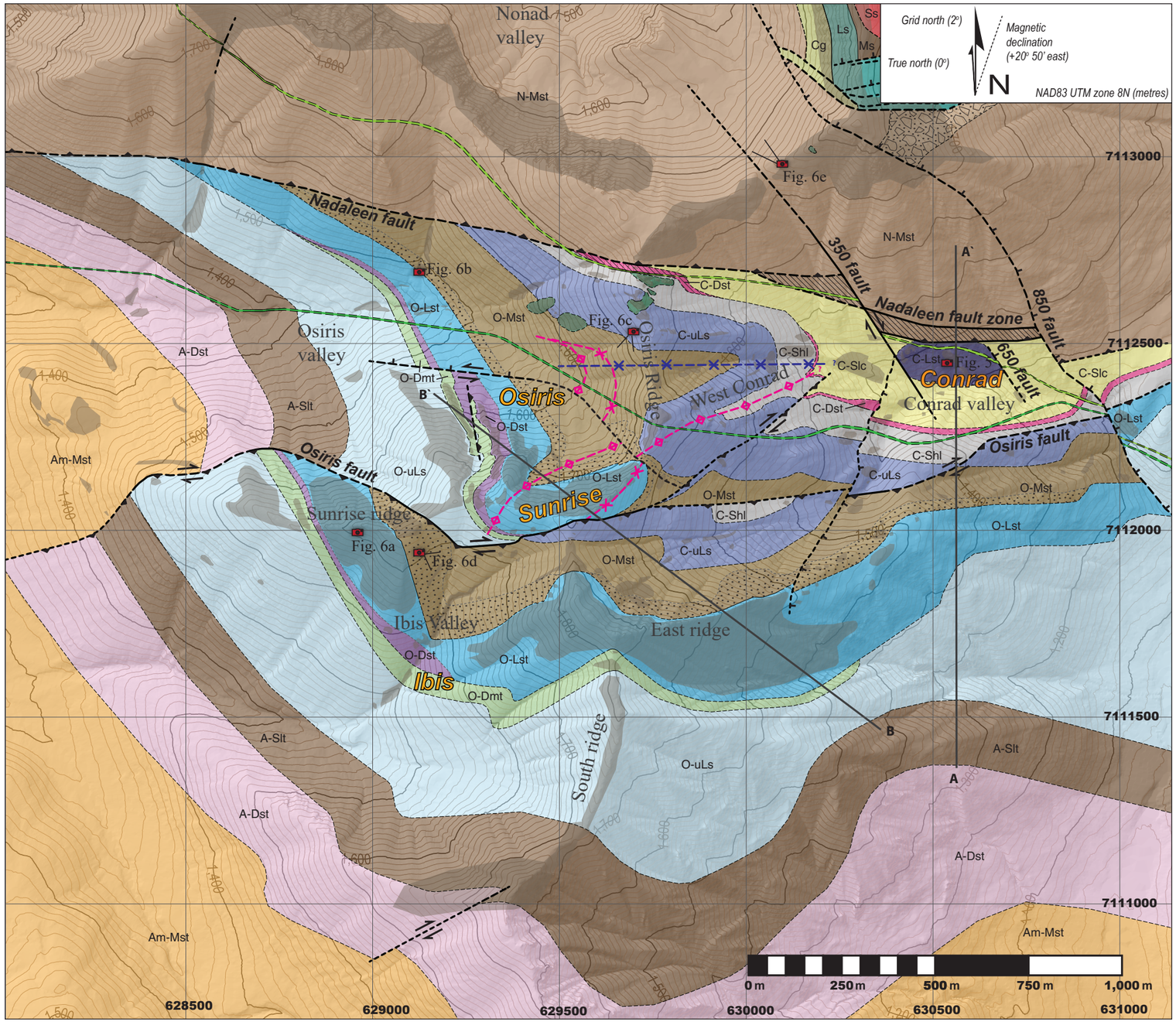

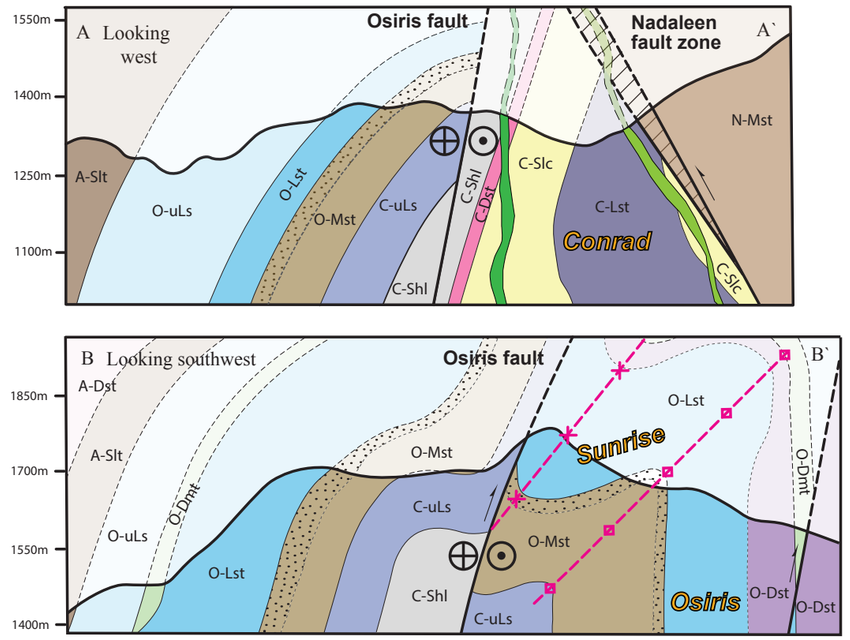

No vertical exaggeration, map scale equal to figures 2a and 2b

Figure 2. *Geology map of the Osiris cluster with geographical names, major fold axial traces, cross section lines and the Osiris, Sunrise, Ibis and Conrad ore zones indicated, and cross sections. Geologic map with overlay showing structural measurements and stereonets and map legend on next page.*

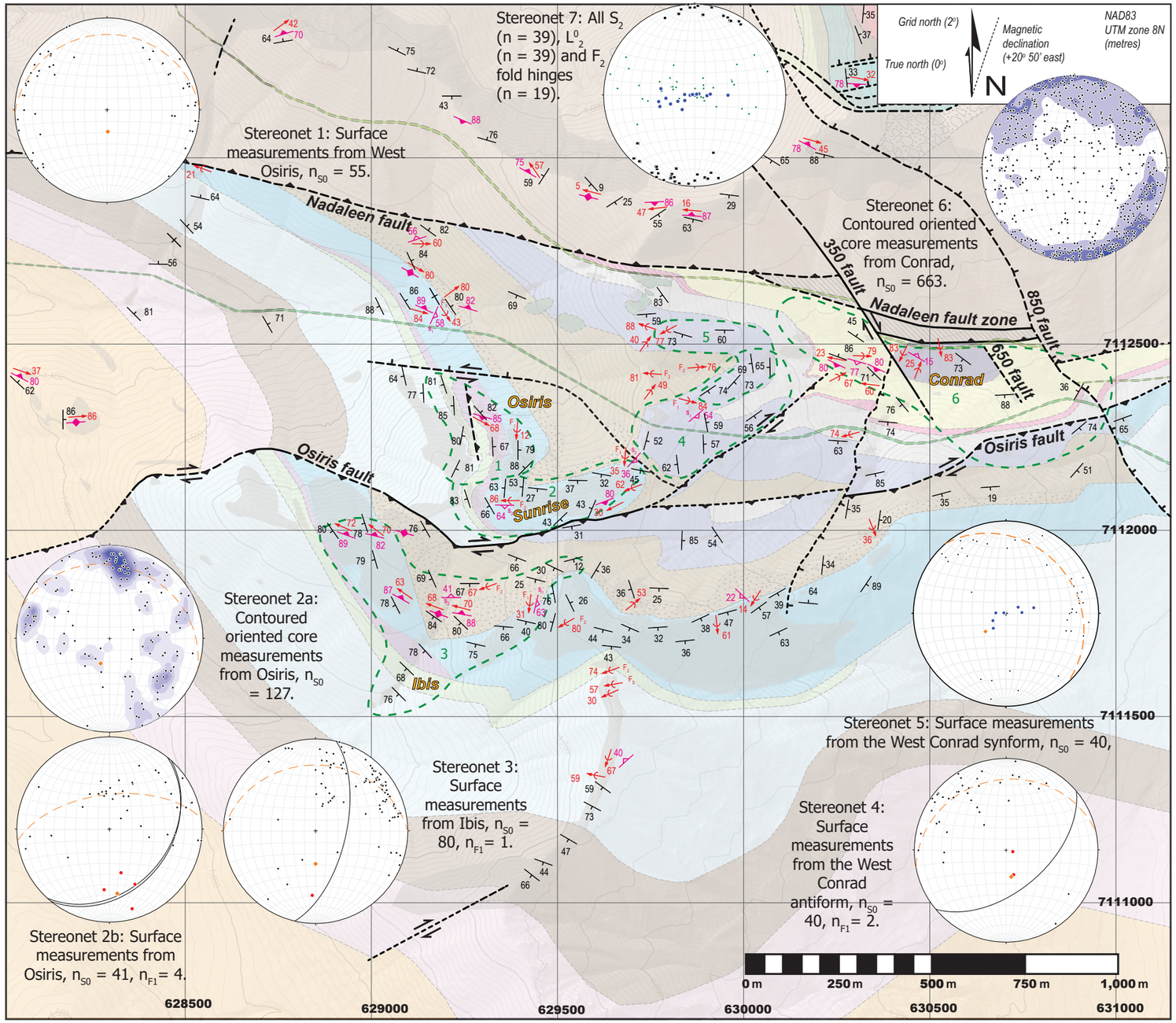

Stereonet symbols

- Area from which data on corresponding stereonet was obtained
- Calculated best fit girdle
- F_1 axial plane
- Pole to S_0
- F1 fold axis
- F2 fold axis
- Pole to best fit girdle
- Pole to S2
- Intersection axis, L02

MAP UNITS

Ediacaran - Cambrian
Narchilla Formation

Amon mudstone, Am-Mst. Grey and maroon thinly bedded mudstone with thicker interbeds of siltstone and fine sandstone.

Ediacaran - Algae Formation

Atum dolostone, A-Dst. Cream to light grey silty or sandy dolostone with minor rudstone interbeds.

Ediacaran - Blueflower Formation

Atum siltstone, A-Slt. Thinly bedded to laminated brown siltstone with interbeded sandy limestone.

Upper Osiris limestone, O-uLs. Thinly bedded sandy limestone with calcareous breccias and rare sandstone interbeds. Distinctive terracotta colour. Readily frost-heaved and creeped.

Ediacaran - Gametrail Formation

Osiris diamictite, O-Dmt. Orange weathering, generally recessive carbonate breccia. Angular clasts of dolostone and limestone supported in a carbonate matrix which is locally dolomitized.

Osiris dolostone, O-Dst. Dolomitized version of Osiris Limestone (see below).

Osiris limestone, O-Lst. Variably bedded and laminated limestone, flat-pebble rudstone and carbonate breccia, often partially dolomitized. Dolomitic beds weather orange while limestone beds weather pale grey. Dark grey when fresh with extensive stylolites. Limestones are silty and locally show manganese dentritic weathering. Abundant soft-sediment deformation. Maroon coloured at its base.

Ediacaran - Nadaleen formation

Osiris mudstone, stippled where maroon coloured. O-Mst. Grey, thinly bedded mudstone and siltstone. Alternating maroon and green coloured layers at top generally follow bedding. Often pencil fractured with small scale folds.

Upper Conrad limestone, C-uLs. Interbedded calcareous breccia, limestone and siliclastic shale. Breccias comprise gravel to cobble sized limestone clasts thatfine upwards in a limestone matrix. Extensive 'beefy' calcite veining.

Conrad shale, C-Shl. Recessive grey to black shale with abundant small scale folds.

Conrad dolostone, hatched where not dolomitised, C-Dst. Pale grey silica dolostone cut by abundant black quartz veins. Not fully dolomitized near Nadaleen fault.

Conrad siliciclastics, C-Slc. Chaotic, interbedded sandstone, mudstone, siltstone and gravel conglomerates. Conglomerates are matrix supported, irregular and lensoidal. Minor calcareous sandstones. Abundant soft-sediment deformation.

Conrad limestone, C-Lst. Thinly bedded silty limestone. Abundant calcite veins and stylolites. Dark-grey weathering and black when fresh. Abundant soft-sediment deformation. Minor dolomitized zones.

Cryogenian - Ice Brook Formation

Unclassified Nonad mudstone, patterned where diamictite, N-Mst. Interbedded mudstone and siltstone with minor sandstone. Large rafts of dolostone and conglomerate. Weathers along S2. Abundant soft-sediment deformation. Diamictites are polymict with clasts of sandstone, mudstone and limestone supported in a blue-grey clay matrix.

Upper sandstone, Ss. Poorly sorted, generally coarse grained orange-weathering sandstone.

Upper mudstone, Ms. Dark grey to black laminated claystone and siltstone.

Nonad limestone, Ls. Dominantly grey granular limestone with isolated coarse quartz clasts. Buff-weathering. Interbedded with trough cross-bedded siltstone and black mudstone.

Cryogenian - Twitya Formation

Quartz gravel conglomerate, Cg. Locally with minor feldspar clasts. Interbedded with sandstone and black mudstone.

Intrusive rocks

North Conrad dike. Altered mafic dike. Pale grey when fresh and orange weathering. 74.4Ma (Tucker, 2015).

South Conrad dike. Altered mafic dike. Pale grey-green when fresh and orange weathering. 74.4Ma (Tucker, 2015).

Osiris gabbro. Altered hornblende-rich gabbro. Green colour when fresh, black weathering. 465.6Ma (Tucker, 2015).

Fault rocks

Nadaleen fault zone. Sheared cataclasite comprising clasts from the Nonad mudstone, Conrad siliciclastics and Conrad limestone.

Map symbols

- Observed contact
- Inferred contact
- Exposure
- Fault - observed
- Fault - approximate location
- Fault - inferred
- Reverse motion - triangles on up-thrown block
- Normal motion - ticks on down-thrown block
- Lateral motion
- F1 axial trace (syncline)
- F_1 axial trace (anticline)
- F_2 axial trace (syncline)
- Photo location for figures
- Strike and dip of inclined bedding
- Strike of vertical bedding
- Strike and dip of inclined cleavage (S_2)
- Strike of vertical cleavage (S_2)
- Plunge and trend of bedding-cleavage intersection lineation (L^0_2)
- Strike and dip of axial plane (S1)
- Strike and dip of axial plane (S2)
- Strike and dip of axial plane (unknown or syn-sedimentary fold)
- Plunge and trend of minor fold axis (F1)
- Plunge and trend of minor fold axis (F2)
- Plunge and trend of minor fold axis (unknown or syn-sedimentary fold)

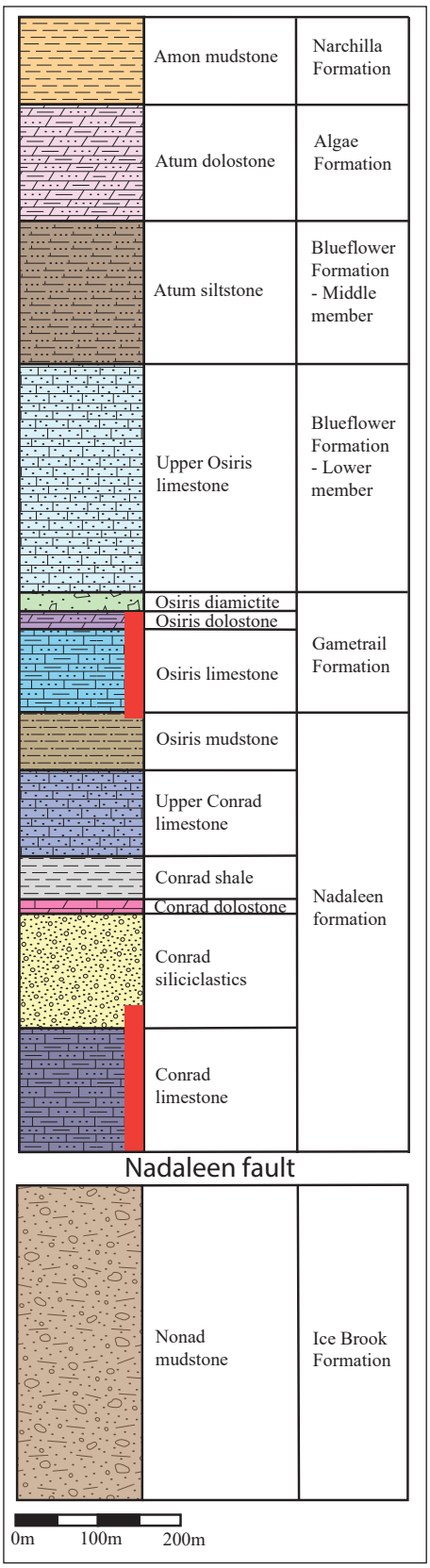

Figure 3. *Stratigraphic succession of sedimentary rocks in the Osiris cluster. Mineralized intervals are shown in red. Regional correlation is after Moynihan (2016).*

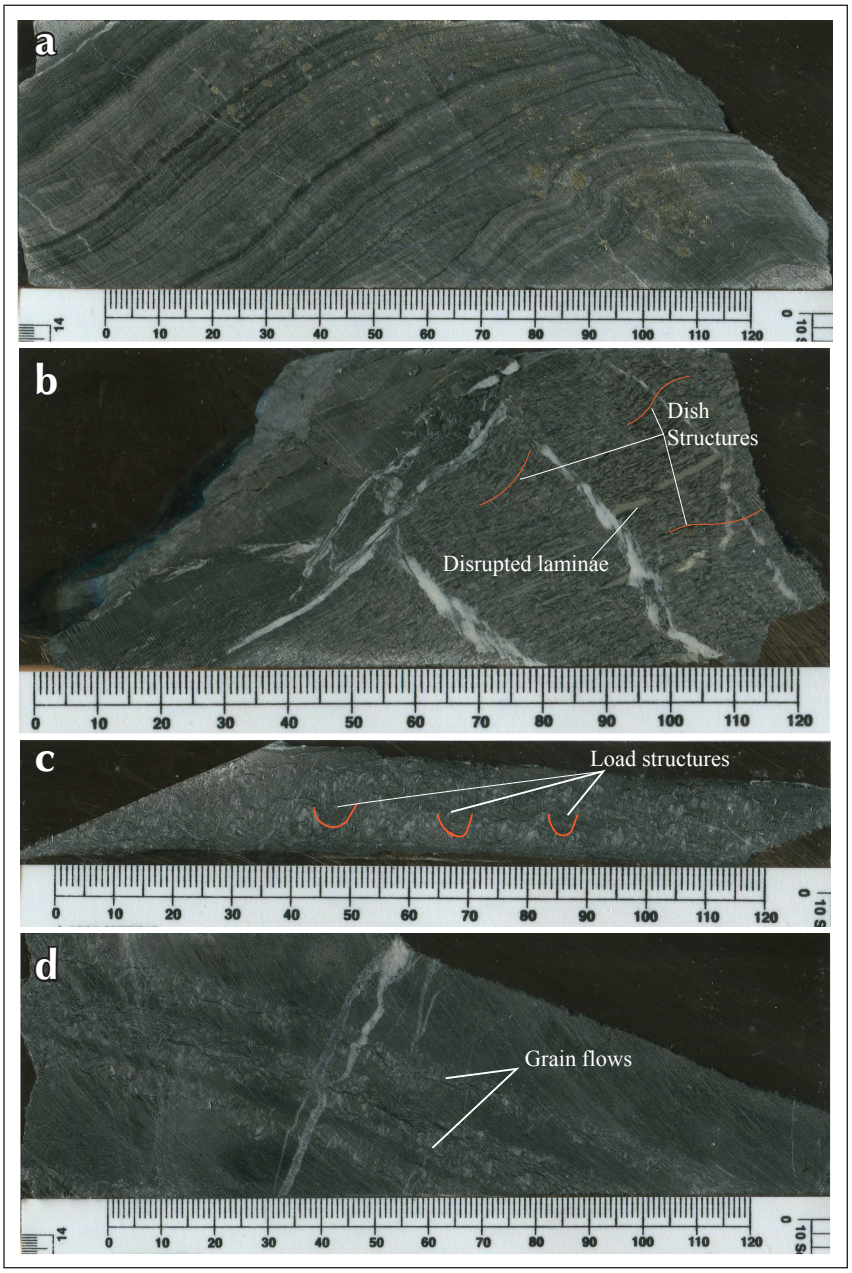

Figure 4. *Core photographs of sedimentary structures in the Conrad limestone.* ***(a)*** *Synsedimentary folding;* ***(b)*** *interrupted laminae with dish structures;* ***(c)*** *convoluted bedding with small-scale slumps and load casts; and* ***(d)*** *grain flows with interrupted laminae. Scale in millimetres.*

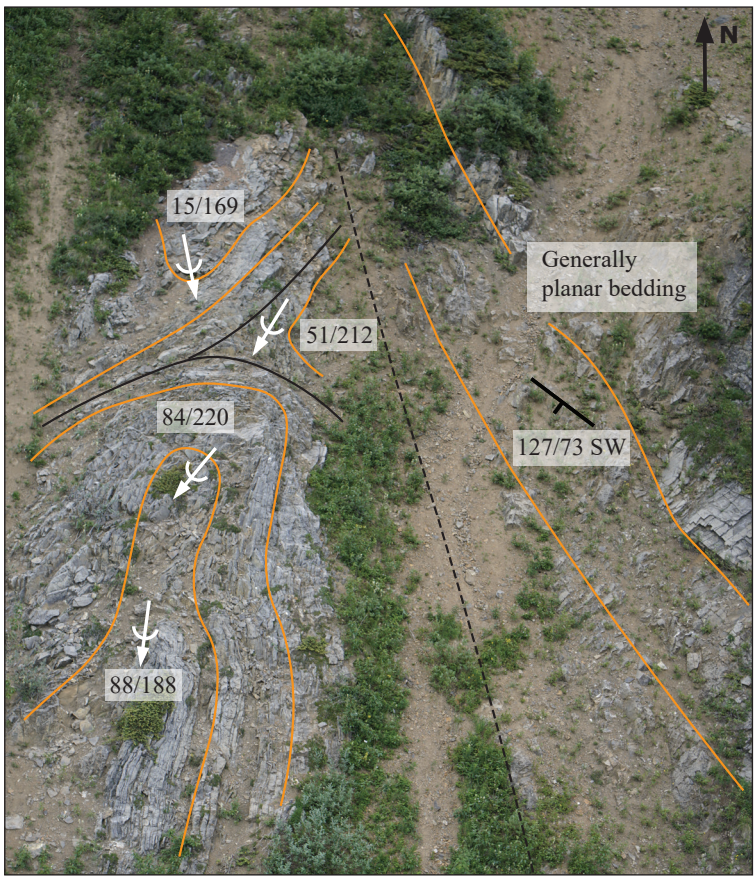

Figure 5. *Annotated oblique aerial view of a steep exposure of Conrad limestone with interpreted soft-sediment slump folds. Bedding formlines are represented in orange whereas black lines represent observed (solid) or inferred (dashed) truncation surfaces. Fold hinges (shown in white) are denoted by plunge/trend and a representative value for generally homoclinal bedding to the east is in the form strike/dip/dip direction. Note the variance in fold hinge plunge. Field of view is ~12 m across.*

STRUCTURAL GEOLOGY

FOLIATIONS

A well-developed S_2 foliation is present in all argillaceous rocks and is locally developed in limestone units (Fig. 6a). This fabric is best observed along the western extent of the Sunrise ridge within the Osiris limestone (629000 mE, 7112010 mN), and in the Ice Brook Formation immediately north of the Nadaleen fault where the foliation forms a prominent weathering surface. S_2 strikes ESE with a subvertical dip and has been recognized throughout the Orion area and elsewhere regionally (Moynihan, 2014), suggesting it can serve as a regional marker foliation. S_2 is axial planar to vertically plunging F_2 folds (described below; Fig. 6b) and crosscuts macro scale F_1 folds. Across the Osiris cluster, intersection lineations of S_2 with bedding exhibit considerable variation in plunge (Fig 2b; Stereonet 7), indicating pre-F_2 folding occurred on a large scale. No S_1 fabric was identified in the field, although the intersection of S_2 and a weakly developed bedding parallel fissility has resulted in pervasive conchoidal pencil fracturing of argillaceous rocks and this commonly obscures the identification of any potential pre-S_2 fabrics.

FOLDING

Two phases of mesoscopic to macroscopic folding have affected the Osiris cluster. F_1 folds are primarily developed on the macroscopic scale with the Osiris antiform-synform fold pair (Fig. 6c), and the West Conrad anticline being the most prominent examples of large F_1 folds in the Osiris cluster. F_1 folds have a steep to moderate southerly plunge and steep to moderately southeast-dipping axial planes. Where least affected by F_2 folding, these large F_1 folds typically have one subvertically dipping limb and one shallow to moderate dipping limb (*e.g.*, the Osiris antiform-synform fold pair, Fig. 6c). Although parasitic mesoscopic F_1 folds are not common, they can be readily observed adjacent to the Osiris ridge (629700 mE, 7112185 mN) and in the Ibis valley (629440 mE, 7111800 mN). Comparable scale F_1 folds are also observed in the Mississippian limestone in the Orion area.

F_2 folds overprint F_1 folds and are characterized by axial planes that dip steeply to the south. S_2 is typically developed as an axial plane foliation to F_2 folds (Fig. 6b). Mesoscopic F_2 folds are well developed on the Sunrise ridge (629325 mE, 7112075 mN), and along the Osiris ridge and at West Conrad. Examples of macroscopic F_2

folds are the West Conrad synform and the West Osiris synform (Fig. 2, Stereonets 1 and 5). The F_2 fold axes and intersection lineations between bedding and S_2 vary from a shallow to steep plunge within S_2 (Fig. 2, Stereonet 7). The most prominent examples of F_2 folds have a steep to subvertical plunge that likely represent folding of the steeply dipping limbs of macroscopic F_1 folds.

In the Ibis valley and along the East ridge, subhorizontal upright monoclinal warps in bedding are developed on a macroscopic scale (Fig. 6d; cross sections in Fig. 2). A similar monoclinal warp is evident in drill core through the Sunrise zone (Fig. 2, Stereonet 2a). The dominant bedding attitude at depth is steep to the south, compared to a 30-40° southerly dip at the surface (Fig. 2, Stereonet 2b). The monocline overprints the Osiris antiform-synform F_1 fold pair and is interpreted as being a product of F_2 folding of an F_1 shallow limb. An upright subhorizontal macroscopic F_2 fold can be observed on the western bluffs of the Nonad valley (Fig. 6e). Similar upright, subhorizontal, open to close folds that we interpret as being F_2 structures can be recognized on regional maps (Moynihan, 2016; Colpron, 2012) and are particularly clear in aerial photographs of the Orion area. The regions characterized by shallow plunging F_2 monoclines and F_2 folds likely represent folding of shallow dipping F_1 fold limbs and/or regions largely unaffected by F_1 folding.

Palmer and Kuiper (2017) identified a macroscopic antiform in the Ibis area. This fold was mapped as having a steep SE-dipping limb and a steep SW-dipping limb, but this is inconsistent with field observations made in this study (Fig. 2, Stereonet 3). Our data indicate the fold is an open antiformal flexure with a gentle interlimb angle of greater than 130°. We interpret this as being an F_1 structure and we correlate it with the Osiris antiform on the north side of the Osiris fault (*see* below). We suggest that the tighter 'fold-shaped' map pattern at Ibis is largely a function of shallow topography near the Osiris fault owing to the presence of an F_2 monocline (Fig. 6d) and the interaction with topography creating a pronounced 'V-in-the-valley' (Fig. 2).

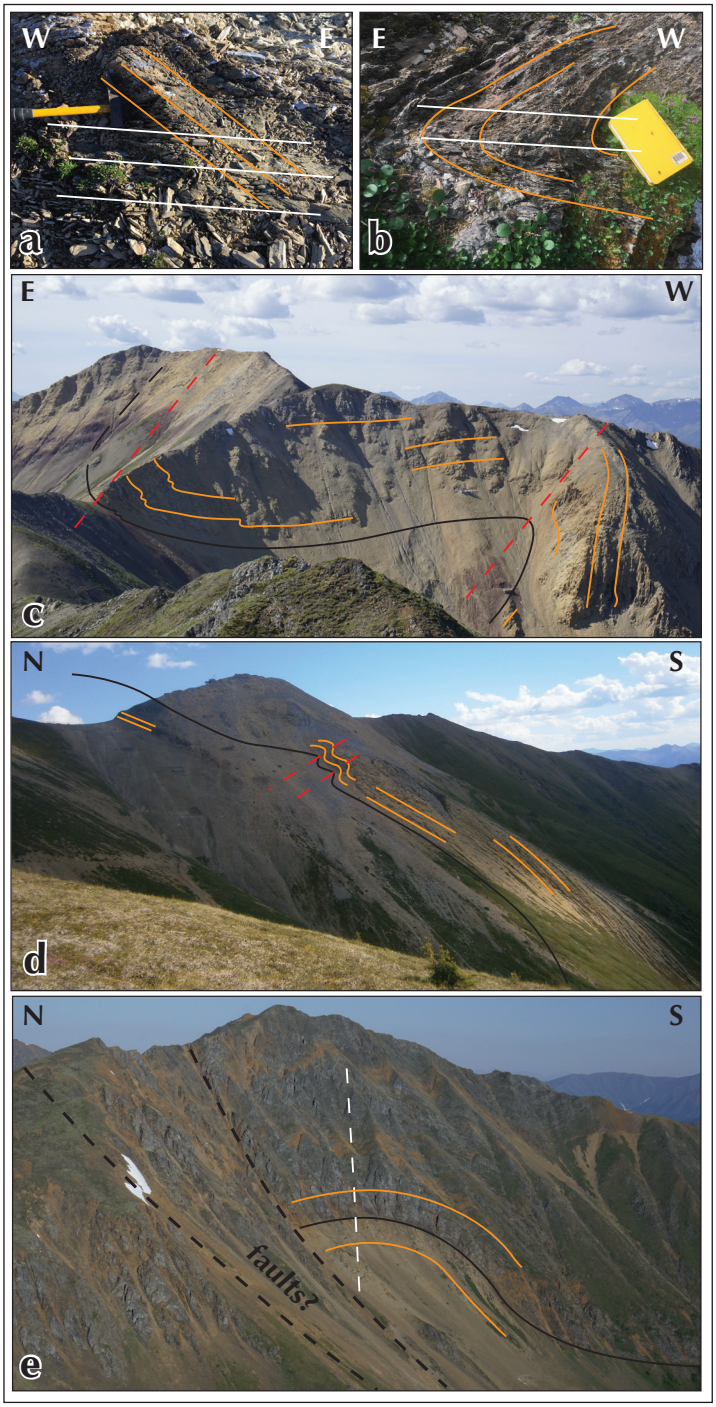

Figure 6. *Annotated field photographs. Bedding formlines are shown in orange, unit contacts in black, faults in dashed black, F_1 axial traces in red dashed, S_2 cleavage in white and F_2 axial traces in dashed white. Photo locations shown in Figure 2.* ***(a)*** *Bedding-cleavage on Sunrise ridge. Hammer shaft is 37 cm;* ***(b)*** *S_2 axial planar to an F_2 fold. Notebook spine is 19 cm;* ***(c)*** *Osiris F_1 antiform-synform pair. Wavelength pictured is ~325 m;* ***(d)*** *F_2 monocline at Ibis. Field of view is ~650 m across; and* ***(e)*** *upright F_2 fold hinge, Nonad valley. Field of view is ~500 m across.*

FAULTS

The Osiris cluster is cut by a number of significant faults that generally strike E, W or NW. The largest fault in terms of lateral extent is the Nadaleen fault, which can be traced west at least as far as the Pyramid gold showing, approximately 16 km west of the Osiris cluster (Fig. 1b; Moynihan, 2016). It has a net reverse displacement, placing Cryogenian rocks of the Ice Brook Formation on top of Ediacaran rocks within the Osiris cluster, where it strikes WNW. In Orion, it strikes NW and juxtaposes Paleozoic rocks to the south against Ediacaran rocks to the north. Drilling in the Conrad zone has constrained the Nadaleen fault to dip 60° to the north and also identified a large brittle shear zone known as the Nadaleen fault zone. This is a zone of sheared cataclasite, 60 m wide at its thickest, which occurs approximately between the 350 and 650 faults. Drill core data from Conrad indicate that there is no increase in thickness of sedimentary units towards the fault plane, nor are any rollover structures developed. As such, we suggest the Nadaleen fault did not initiate as a synsedimentary structure. Rather, it initiated after the deposition of these rocks constraining its age to Paleozoic or younger. The Nadaleen fault is not folded and is interpreted to cut all folds.

The other large fault within the study area is the Osiris fault, which is an E striking structure that cuts through the centre of the Osiris cluster (Fig. 2). Drill core data from the Sunrise ore zone indicates that the fault dips to the south at ~70°, although its strike varies significantly along its length. Correlation of the anticlinal flexure at Ibis in the hanging wall to the fault with the Osiris antiform in the footwall, constrains net slip on the fault to have been oblique, with a dextral-reverse sense. The Sunrise zone of gold mineralization forms a plane that is subparallel to the Osiris fault, but is offset ~50 m down into the footwall. Drill core through the Osiris fault and the Sunrise zone define a continuous brittle shear zone comprising intensely fractured rock, fault gouge, sheared material and high vein density between them suggesting that the Sunrise zone might represent fluid flow through the high–permeability damage zone on the periphery of a wide, multi-cored Osiris fault zone (Faulkner *et al.,* 2010). The Osiris fault cuts both F_1 and F_2 folds, restricting its age to post-folding.

The other dominant orientation of faults in the Osiris cluster are the NW-striking 350, 650 and 850 faults. These structures were targeted by diamond drilling for the first time in the summer of 2017. All three faults are spatially associated with mineralization and are interpreted as potential fluid conduits during mineralization. The 350 fault has a dextral strike separation in plan view while the 650 and 850 faults have an apparent normal offset to the east. Drill data indicate displacement of both Conrad dikes across the 350 fault, indicating post-74.4 Ma slip. Drilling has not yet identified any significant offset across the 650 or 850 faults.

INTERNAL GEOMETRY OF THE CONRAD LIMESTONE

Extensive diamond drilling in the Conrad ore zone has shown that the Conrad limestone has a 3D lenticular geometry with depth; the strike length and unit thickness both decrease upwards as it approaches the Nadaleen fault (*see* cross section A-A`; Fig. 2). It is also bound on either side by a siliciclastic package that is thought to represent the same stratigraphic horizon - the Conrad siliciclastic unit. One possible explanation for this geometry is that the Conrad limestone is the core of an upright anticline, with a subvertical E-striking axial plane that is double plunging to the east and west (ATAC Resources Ltd., 2017). This geometry is anomalous in the wider tectonic context as it requires a tight interlimb geometry that is not observed in macroscopic folds elsewhere.

We propose that the Conrad limestone is an olistostrome and that its geometry is primarily a function of its emplacement morphology. We infer this from the abundance of slump folding and soft-sediment deformation within the Conrad limestone (Figs. 4 and 5), the inconsistency between structural measurements and outcrop pattern (Fig. 2; Stereonet 6), and the repeated Conrad siliciclastic unit on either side of the Conrad limestone. Furthermore, the Conrad limestone is not correlated with any part of the Nadaleen formation elsewhere regionally (Moynihan, 2016). The apparent double plunging nature of the Conrad limestone is a function partly of its lenticular emplacement shape and apparent normal dip-slip motion along the 650 and 850 faults that cut across it. As an olistostrome, the Conrad limestone would have been emplaced during deposition of the Conrad siliciclastics. The provenance of the Conrad limestone is currently unknown.

FOLD EVOLUTION

The geometry of various parts of the Osiris cluster can be explained using the following fold evolution model (Fig. 7). NW-SE directed bulk shortening produced NW-verging F_1 folds with a subvertical limb and a shallow limb (Fig. 7a,b). This was later refolded in response to SSW-NNE directed contraction (Fig. 7b). F_2 folds formed with S_2 as an axial planar cleavage. In steep F_1 limbs, these folds have subvertical plunges while in shallow limbs they have subhorizontal plunges and form large wavelength monoclines, although upright F_2 hinges are observed elsewhere regionally. F_1 folds hinges were steepened towards the south (Fig. 7c). Folding is cut by both the Osiris fault and the Nadaleen fault, indicating that these faults likely formed post-folding. However, they may be longer-lived structures that were recurrently active during folding. Later NW striking faults in the Conrad ore zone are spatially associated with mineralization and, if they all developed contemporaneously with the 350 fault, are constrained to post dike emplacement at 74.4 Ma. This model is consistent with observations by Palmer and Kuiper (2017), who proposed a similar model in which SSW-directed tilting came prior to folding and justified this with the lack of evidence for a prior E-W fold event elsewhere. We propose that the observations outlined in this contribution are evidence for such a prior event, at least locally.

FUTURE WORK

This study forms the structural context within which ore fluid pathways into, out of, and within the Nadaleen trend will be assessed. Future work will focus on mapping fluid conduits using isotopic, thermal and mineralogical proxies for fluid alteration including $\delta^{18}O$ isotopes, clumped isotopes, apatite fission track thermochronology and illite crystallinity. The aim is to recognize fluid pathways on three scales: 1) identifying where fluids enter and exit the Nadaleen trend as a whole; 2) assessing the macroscopic structures controlling the distribution of ore zones; and 3) identifying small scale structures (stylolites, veins, minor faults) that are fluid conduits into mineralized horizons. This will be coupled with additional structural studies, including investigation of fault kinematics, analysis of fabrics in oriented thin-sections and assessing deformation age constraints through geochronology of intrusive rocks.

Understanding the deformation context in which ore fluid pathways formed will help identify possible mineralizing structures elsewhere and explain the distribution of mineralized zones.

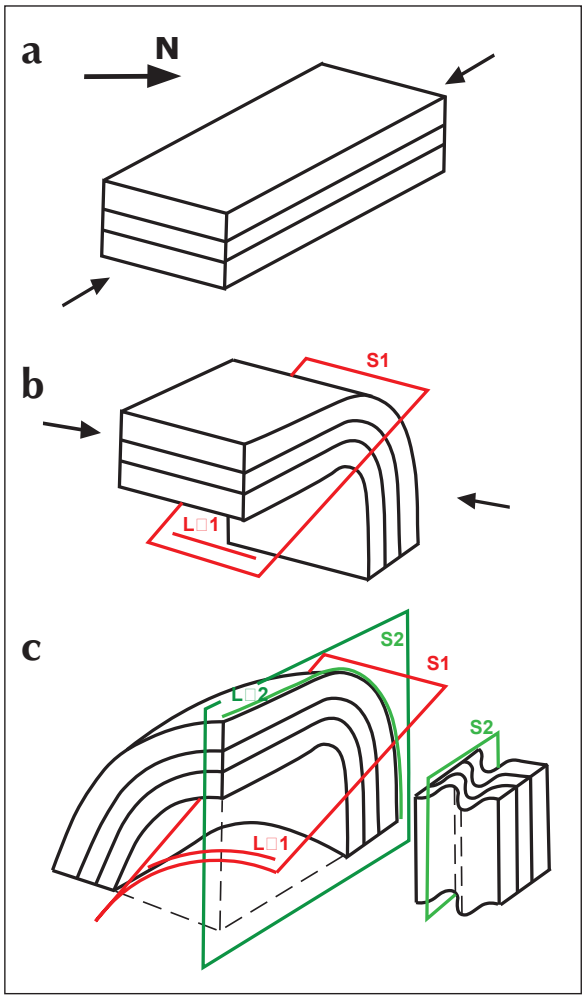

Figure 7. *Fold evolution within the Osiris cluster.* ***(a)*** *NW-SE directed contraction of subhorizontal beds;* ***(b)*** *Formation of F_1 folds with a shallow limb, steep limb and an axial plane shown in red. L^0_1 is the intersection lineation of S_0 and S_1. Later NNE-SSW directed compression; and* ***(c)*** *refolding of F_1 folds. Shallow limbs are refolded into F_2 monoclines while steep limbs are refolded to steeply plunging F_2 folds with subvertical south-dipping axial planes (shown in green). L^0_1 is folded so that it has a variable plunge towards the south. L^0_2 is the intersection lineation of S_0 and S_2.*

ACKNOWLEDGEMENTS

This work was conducted as part of Andrew Steiner's MSc thesis at the University of British Columbia. We would like to thank Julia Lane of ATAC Resources Ltd. for all of her logistical support, Daniel Schrader for his assistance in the field, and to Barrick Gold Corporation for their expertise and support during a busy field season. This project is funded by Natural Resources Canada through their Targeted Geoscience Initiative (TGI), the Mitacs Accelerate Program, the Society of Economic Geologists Foundation's Graduate Student Fellowship and ATAC Resources Ltd. Thank you to Jim Mortensen and Patrick Sack for their feedback when reviewing this paper.

REFERENCES

Aitken, J.D., 1989. Uppermost Proterozoic formations in central Mackenzie Mountains, Northwest Territories. Geological Survey of Canada, Bulletin 368.

Aitken, J.D., 1991. The Ice Brook Formation and Post-Rapitan, Late Proterozoic glaciation, Mackenzie Mountains, Northwest Territories. Geological Survey of Canada, Bulletin 404.

ATAC Resources Ltd., 2017. Osiris Project. http://www.atacresources.com/projects/rackla/osirus-cluster [accessed 26th Nov. 2017].

Bradley, D. and Hanson, L., 1998. Paleoslope Analysis of Slump Folds in the Devonian Flysch of Maine. The Journal of Geology, vol. 106, p. 305-318.

Colpron, M., 2012. Preliminary observations on the geology of the Rackla belt, Mount Ferrell map area (NTS 106C/3), central Yukon. *In:* Yukon Exploration and Geology 2011, K.E. MacFarlane and P.J. Sack (eds.), Yukon Geological Survey, p. 27-43.

Colpron, M., Moynihan, D., Israel, S., and Abbott, G., 2013. Geological map of the Rackla belt, east-central Yukon (NTS 106C/1-4, 106D/1). Yukon Geological Survey, Open File 2013-13, 1:50 000 scale, 5 maps and legend.

Colpron, M. and Nelson, J.L., 2011. A Digital Atlas of Terranes for the Northern Cordillera. Accessed online from Yukon Geological Survey, www.geology.gov.yk.ca [accessed 26th Nov. 2017].

Coulter, A. B., Lane, J. and Steiner, A., 2018. Osiris cluster Carlin-type gold, east-central Yukon. *In:* Yukon Exploration and Geology 2017, K.E. MacFarlane (ed.), Yukon Geological Survey, p. 65-74.

Faulkner, D.R., Jackson, C.A.L., Lunn, R.J., Schlische, R.W., Shipton, Z.K., Wibberley, C.A.J. and Withjack, M.O., 2010. A review of recent developments concerning the structure, mechanics and fluid flow properties of fault zones. Journal of Structural Geology, vol. 32, p. 1557-1575.

Moynihan, D., 2014. Bedrock Geology of NTS 106B/04, Eastern Rackla Belt. *In:* Yukon Exploration and Geology 2013, K.E. MacFarlane, M.G. Nordling, and P.J. Sack (eds.), Yukon Geological Survey, p. 147-167.

Moynihan, D., 2016. Bedrock geology compilation of the eastern Rackla belt, NTS 105N/15, 105N/16, 105O/13, 106B/4,106C/1,106C/2, east-central Yukon. Yukon Geological Survey, Open File 2016-2, 1:75 000 scale.

Palmer, J.C. and Kuiper, Y.D., 2017. Structural geology of the eastern Nadaleen trend, Yukon Territory, Canada: Implications for recently discovered sedimentary rock-hosted gold. Ore Geology Reviews, vol. 80, p. 48-60.

Tucker, M.J., 2015. Geology, Mineralization and Geochronology of the Conrad Zone Carlin-type gold prospect, East-Central Yukon Territory, Canada. Unpublished MSc thesis, University of British Columbia, 213 p.

Tucker, M.J., Hart, C.J.R. and Carne, R.C., 2013. Geology, alteration, and mineralization of the Carlin-type Conrad zone, Yukon. *In:* Yukon Exploration and Geology 2012, K.E. MacFarlane, M.G. Nordling, and P.J. Sack (eds.), Yukon Geological Survey p. 163-178.